Photonics and Optoelectronics

Effects of Line Edge Roughness on Photonic Device Performance through Virtual Fabrication

S. I. El-Henawy, D. S. Boning
Sponsorship: AIM Photonics

Silicon photonics has garnered a large amount of interest in recent years due to its potential for high data transfer rates and for other, more novel applications. One attractive feature of silicon photonics is its relatively seamless integration with existing CMOS fabrication technologies. That means, however, that it is subject to similar random and systematic variations as are known to exist in CMOS manufacturing processes.

One common source of process variation is Line Edge Roughness (LER), which occurs during lithography. Since LER produces random perturbations to the component geometry, it is likely to influence the light-guiding abilities of photonic components and devices subject to LER.

We study the effect of LER on the performance of a fundamental component, the Y-branch, through virtual fabrication simulations (Figure 1). Ideally, the Y-branch transmits the input power equal to its two output ports. However, imbalanced transmission between the two output ports is observed when LER is imposed on the Y-branch (Figure 2) depending on the statistical nature (amplitude and correlation length) of the LER. The imbalance can be as low as 1% for small LER amplitudes, and reach up to 15% for large LER amplitudes (Figure 3). These results can be captured as worst-case corner models and included in variation-aware photonic compact models.

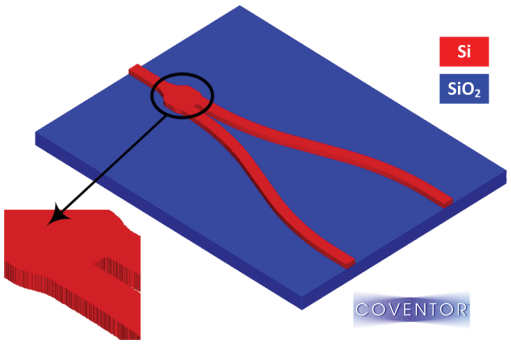

▲ Figure 1: Overview of the Y-branch geometry. Inset: Closeup view showing line edge roughness applied to the Y-branch.

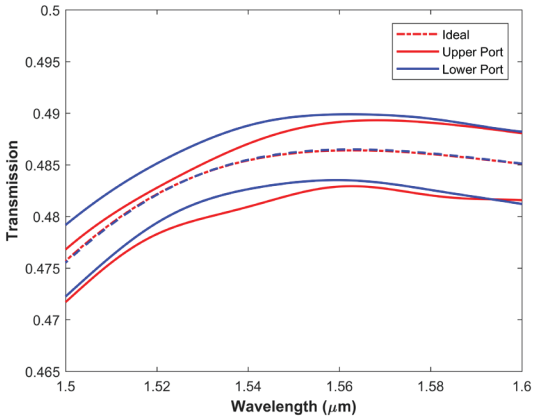

▲ Figure 2: Power splitting between the two output ports of the Y-branch. The dashed lines represent the ideal (no LER) case and the solid lines represent one LER case.

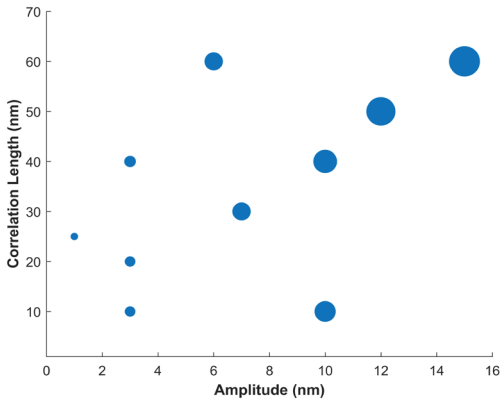

▲ Figure 3: Relative imbalance (size of bubble) in Y-branch transmission as a function of LER amplitude and correlation length.

FURTHER READING

- L Chrostowski and M Hochberg, "Silicon Photonics Design: from Devices to Systems," *Cambridge: Cambridge University Press*, 2015.
- D. Malati, A. Melloni, and F. Morichetti, "Real Photonic Waveguides: Guiding Light through Imperfections," *Advances in Optics and Photonics*, vol. 6, no. 2, pp. 156-224, Jun. 2014.
- C. A. Mack, "Generating Random Rough Edges, Surfaces, and Volumes," *Applied Optics*, vol. 52, no. 7, pp. 1472-1480, Mar. 2013.

Reprogrammable Electro-Chemo-Optical Devices

D. Kalaev, H. L. Tuller
Sponsorship: U.S. Department of Energy, Basic Energy Sciences Program

Photonic devices with programmable properties allow more flexibility in manipulation of light. Recently, several examples of reconfigurable photonic devices were demonstrated by controlling the local/overall index of refraction in thin films, either by thermally induced phase change in chalcogenides or by intercalation of lithium into oxides. We propose a novel approach for design of reprogrammable photonic devices based on electrochemical modification of ceria-based electro-chemo-optical devices.

Previously, it was shown that the refractive index of $Pr_xCe_{1-x}O_{2-\delta}$ (PCO) is a function of oxygen nonstoichiometry, δ that can be controlled electrochemically via closely spaced electrodes in a lateral device configuration. For modified transverse configurations, a PCO thin film on yttrium stabilized zirconia (YSZ) substrate with Transparent Conducting Oxide (TCO) top electrode allows for voltage controlled oxygen exchange. Enhanced spatial resolution can be further achieved with the aid of lithographically patterned nano-dimensioned oxide layers.

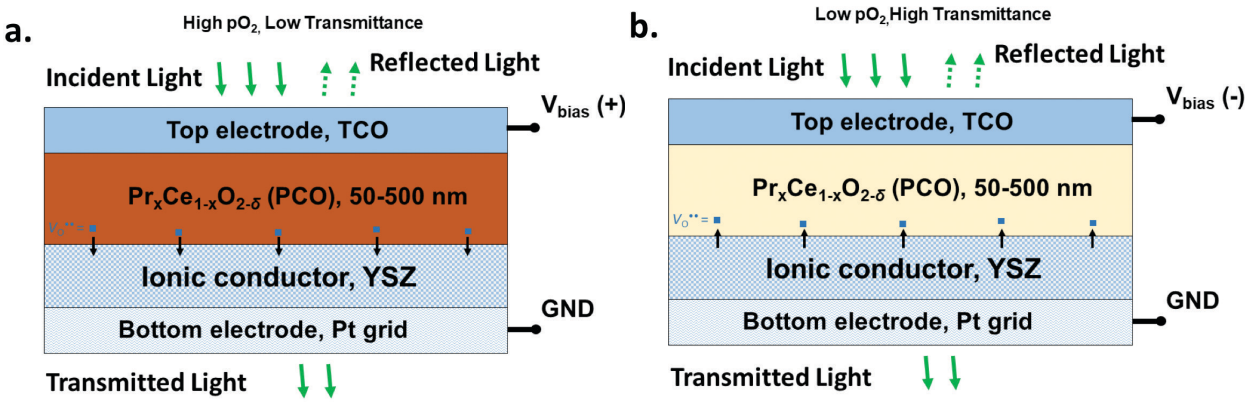

▲ Figure 1: Nonvolatile change in the optical transmission of $Pr_xCe_{1-x}O_{2-\delta}$ (PCO) thin film by electrochemical oxygen pumping. a. Oxygen pumped into the PCO thin film by an applied positive bias, resulting in the low optical transmission. b. Oxygen pumped out of the PCO thin film by an applied negative bias, resulting in the high optical transmission.

On-chip Infrared Chemical Sensor Leveraging Supercontinuum Generation in GeSbSe Chalcogenide Glass Waveguide

Q. Du, Z. Luo, H. Zhong, Y. Zhang, Y. Huang, T. Du, W. Zhang, T. Gu, J. Hu
Sponsorship: DTRA

In this report, we demonstrate the first on-chip spectroscopic chemical sensor with a monolithically integrated supercontinuum (SC) light source. Unlike traditional broadband, blackbody sources used in benchtop Infrared Radiation (IR) spectrophotometers waveguide SC sources feature high spatial coherency essential for efficient light coupling and manipulation on a photonic chip. Compared to tunable lasers, SC offers superior bandwidth coverage. The broadband nature of SC facilitates access to wavelengths that are difficult to cover using semiconductor lasers, and thereby, significantly expands the identifiable molecule repertoire of spectroscopic sensors. In our experiment, we use chalcogenide glass (ChG) as the waveguide material for both SC generation and evanescent wave sensing. ChGs are known for its broadband infrared transparency, large Kerr nonlinearity, and low two-photon absorption (TPA), ideal characteristics for our application.

400 nm thick $Ge_{22}Sb_{18}Se_{60}$ (GeSbSe) films were thermally evaporated onto 4" silicon wafers with 3 µm thermal oxide as an under cladding from GeSbSe glass powders. GeSbSe waveguides with varying length were fabricated using our previously established protocols. In the process, a 350-nm-thick ZEP resist layer was spun onto the substrate followed by exposure on an Elionix ELS-F125 tool at a beam current of 10 nA. The resist pattern was then developed by immersing in ZED-N50 developer for one minute. Reactive ion etching was performed in a PlasmaTherm etcher to transfer the resist pattern to the glass layer. The etching process used a gas mixture of CHF_3 and CF_4 at 3:1 ratio and 5 mTorr total pressure. The incident Radio Frequency (RF) power was fixed at 200 W.

Finally, the device was immersed in N-Methyl-2-pyrrolidone (NMP) overnight to remove the ZEP resist and complete device fabrication. The waveguides assume a zigzag geometry with lengths up to 21 mm. Figure 1a plots the SC spectra in GeSbSe waveguides with the different lengths and the optimal dimensions (W = 0.95 µm, H = 0.4 µm). As indicated in the figures below, the SC bandwidth extends to over half an octave, albeit with decreased total output power when the waveguide length increases to 21 mm. In the sensing experiment, the GeSbSe waveguide was immersed in carbon tetrachloride (CCl_4) solutions containing varying concentrations of chloroform ($CHCl_3$). The CCl_4 solvent is optically transparent across the near-IR, whereas the C-H bond in chloroform leads to an overtone absorption peak centering at 1695 nm, a wavelength outside the standard telecommunication bands. SC spectra near the chloroform absorption peak obtained with GeSbSe waveguides of different lengths are presented in Figure 1b. The data were normalized to the background (collected in pure CCl_4).

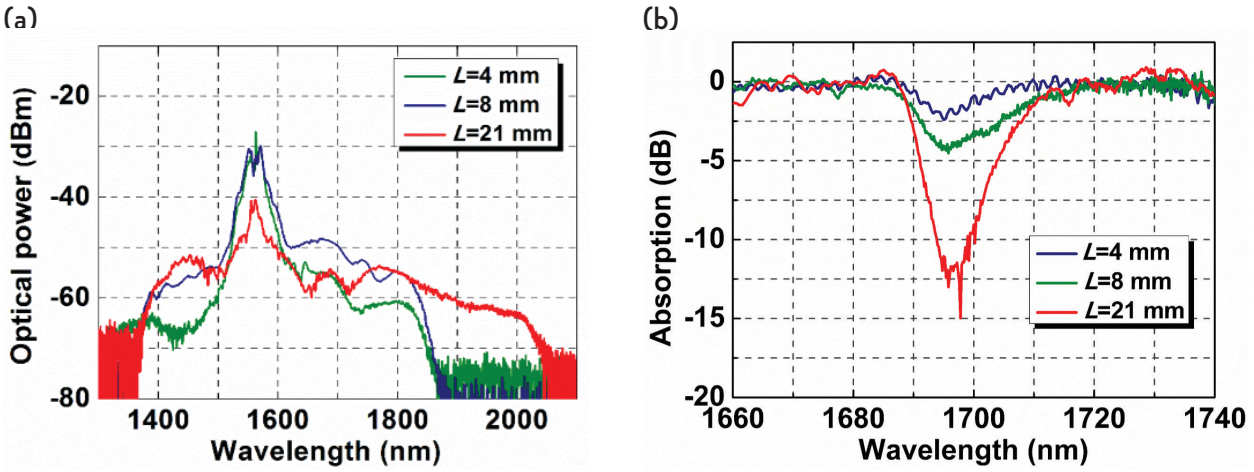

▲ Figure 1 (a) SC spectrum generated from our waveguide; (b) absorption peak of $CHCl_3$ on our sensor chip.

FURTHER READING

- Q. Du, Z. Luo, H. Zhong, Y. Zhang, Y. Huang, T. Du, W. Zhang, T. Gu, and J. Hu, "Chip-scale Broadband Spectroscopic Chemical Sensing using Integrated Supercontinuum Source in Chalcogenide Glass Waveguide," *Photon. Res.*, vol. 6, pp. 506-510, 2018.

Sensing Chemicals in the mid-Infrared using Chalcogenide Glass Waveguides and PbTe Detectors Monolithically Integrated On-chip

P. Su, Z. Han, D. Kita, P. Becla, H. Lin, K. Richardson, L. C. Kimerling, J. Hu, A. Agarwal
Sponsorship: NNSA, DTRA

Chemical sensors are important for many applications, from sensing explosive residues for homeland security and defense to sensing contaminants in air and water for environmental monitoring. However, the sensors currently used for these purposes are either bulky, not very sensitive, or not able to identify a chemical specifically. Integrated photonic sensors, which include a light source, photonic sensing element, and photonic detector integrated directly on-chip, that can operate in the mid-infrared (MIR) chemical fingerprint region, promise to be small, sensitive, and specific chemical sensors. They achieve this by confining light within waveguides packed into a small area and using the evanescent field that exists outside the waveguides to sense the presence of a chemical through absorption spectroscopy, identifying chemicals by their unique absorption spectra. This work focuses on designing and fabricating the first ever MIR integrated sensing element combined with a detector, operating at room temperature.

A spiral waveguide design was chosen for the sensing element due to its long interaction length, which improves sensitivity, while still maintaining a small area footprint. Fabrication was done using a double layer electron beam lithography and liftoff technique to reduce the waveguide sidewall roughness, and therefore loss, of the thermally evaporated chalcogenide glass waveguides. The thermally evaporated polycrystalline PbTe detector was deposited directly underneath the waveguide using photolithography and liftoff. This direct integration of the detector with the waveguide improves coupling of light into the detector while also reducing the size, and therefore noise, level of the detector, allowing it to function at room temperature when most MIR detectors need cooling. Figure 1 shows the spiral sensing element and waveguide integrated PbTe detector. The results from sensing methane gas using 3.3 μm light are shown in Figure 2, demonstrating that this integrated sensing element and detector can effectively sense the presence of chemicals using their MIR absorption spectra.

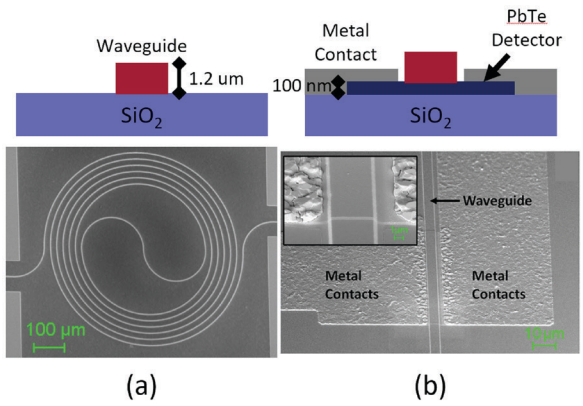

▲Figure 1: Cross-sectional diagrams and SEM images of (a) the spiral sensing element, and (b) the integrated PbTe detector.

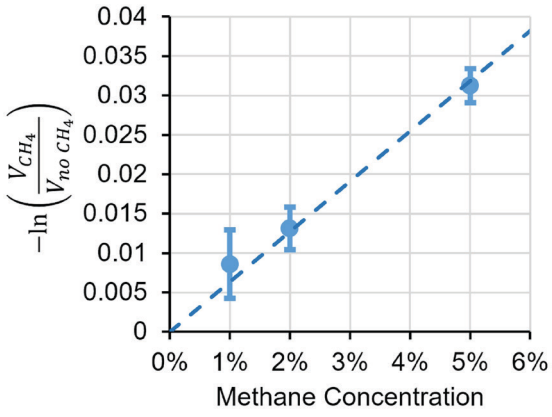

▲Figure 2: The response of the PbTe integrated spiral sensor at known concentrations of methane.

FURTHER READING

- P. Su, Z. Han, D. Kita, P. Becla, H. Lin, K. Richardson, L. C. Kimerling, and J. Hu, et al., "Chalcogenide Glass Waveguide On-chip mid-Infrared Gas Sensor Integrated with PbTe Detector," *American Ceramic Society Glass and Optical Materials Division Meeting*, [presented], San Antonio, TX, May 2018.
- Z. Han, V. Singh, D. Kita, C. Monmeyran, P. Becla, P. Su, J. Li, and X. Huang, et al., "On-chip Chalcogenide Glass Waveguide-integrated mid-Infrared PbTe Detectors," *Applied Physics Letts.*, vol. 109, no. 7, Aug. 2016.
- Z. Han, P. Lin, V. Singh, L. Kimerling, J. Hu, K. Richardson, A. Agarwal, and D. T. H. Tan, "On-chip mid-Infrared Gas Detection using Chalcogenide Glass Waveguide," *Applied Physics Letts.*, vol. 108, no. 14, Apr. 2016.

Broadband Low-loss Nonvolatile Photonic Switches Based on Optical Phase Change Materials (O-PCMs)

Q. Zhang, Y. Zhang, J. Li, R. Soref, T. Gu, J. Hu
Sponsorship: DARPA

Optical switching is an essential function in photonic integrated circuits. Recently, a new class of devices based on O-PCMs have emerged for on-chip switching. Unlike electro-optic or thermo-optic effects which are minuscule, phase transition in O-PCMs generates huge optical property modulation conducive to ultra-compact device architectures. In addition, such phase changes can be non-volatile, exemplified by the transition between amorphous (a-) and crystalline (c-) states in chalcogenide alloys. Despite these attractive features, the performances of existing PCM-based photonic switches are severely compromised by the high optical absorption in traditional O-PCMs.

Here we report the design and modeling of a new kind of photonic switches combining low-loss phase change alloys and a "nonperturbative" design to boost the switching performance. On the one hand, we use a low-loss O-PCM for this application: $Ge_2Sb_2Se_4Te_1$ (GSS4T1). Fig 1a and 1b show the optical constants of GSS4T1 compared with traditional PCM $Ge_2Sb_2Te_5$ (GST225), as measured by ellipsometry. At telecommunication wavelength, the material figure-of-merit, which is defined as index change over extinction coefficient, is 6 times higher. Moreover, the loss of amorphous state GSS4T1 is 0.00017 measured by waveguide cutback method, which is two orders of magnitude lower. On the other hand, the switch design is based on the huge index change of O-PCMs. The basic element is a directional coupler comprised of a bare waveguide (WG1) and a waveguide covered with a PCM strip (WG2). At (a-) state, their indices are matched, and light will be coupler from WG1 to WG2. At (c-) state, due to the large index change of O-PCM, the modal profile will be completely different, and effective index of WG2 will increase a lot so that coupling will not happen. This helps to keep the loss at a low level since light will not travel in WG2 when GSS4T1 is in its (c-) state. Fig 2 and 3 show the state-of-the-art performance of the 1 by 2 and 2 by 2 switches designed by this method.

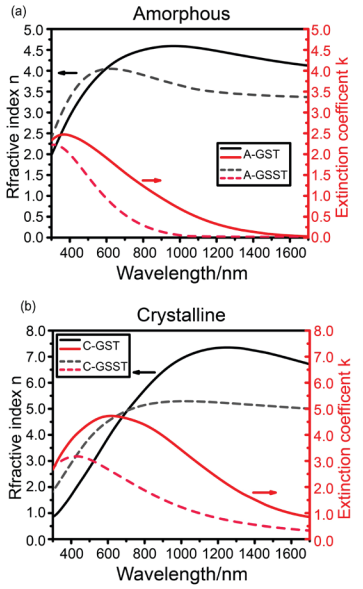

Figure 1

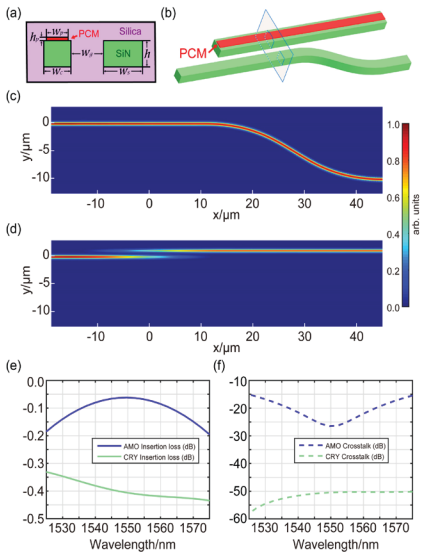

Figure 2

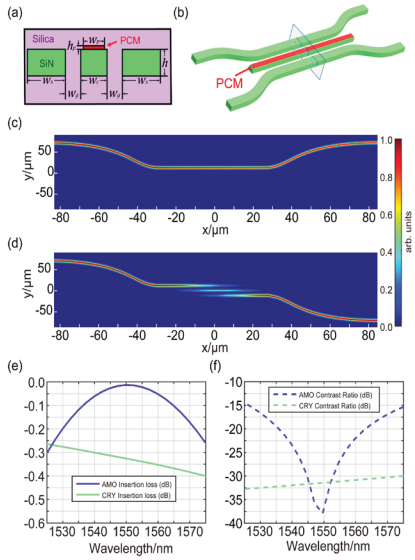

Figure 3

▲ Figure 1: (a, b) optical properties of (a) a- and (b) c- state GSST alloys; Figure 2, 3: (a, b) schematics of structures, (c, d) optical intensity distributions, (e, f) insertion loss and crosstalk of the designed 1 by 2 and 2 by 2 photonic switches.

FURTHER READING

- Q. Zhang, Y. Zhang, J. Li, R. Soref, T. Gu, J. Hu, "Broadband Nonvolatile Photonic Switching Based on Optical Phase Change Materials: Beyond the Classical Figure of-Merit," *Optics Letts.*, vol. 43, no. 1, pp. 94-97, 2018.
- Y. Zhang, J. Li, J. B. Chou, Z. Fang, A. Yadav, H. Lin, and J. Hu, "Broadband Transparent Optical Phase Change Materials," *IEEE Lasers and Electro-Optics (CLEO)*, pp. 1-2, May 2017.

Chalcogenide Glass Waveguide-integrated Black Phosphorus mid-Infrared Photodetectors

S. Deckoff-Jones, H. Lin, D. Kita, H. Zheng, D. Li, W. Zhang, J. Hu
Sponsorship: NSF

Black phosphorus (BP) is a promising 2-D material that has unique in-plane anisotropy and a 0.3 eV direct bandgap in the mid-IR. However, waveguide integrated black phosphorus photodetectors have been limited to the near-IR on top of Si waveguides that are unable to account for BP's crystalline orientation. In this work, we employ mid-IR transparent chalcogenide glass (ChG) both as a broadband mid-IR transparent waveguiding material to enable waveguide-integration of BP detectors and as a passivation layer to prevent BP degradation during device processing as well as in ambient atmosphere.

Our ChG-on-BP approach not only leads to the first demonstration of mid-IR waveguide-integrated BP detectors, but also allows us to fabricate devices along different crystalline axes of black phosphorus to investigate, for the first time, the impact of in-plane anisotropy on photoresponse of waveguide-integrated devices. The best device exhibits responsivity up to 40 mA/W and noise equivalent power as low as 30 pW/Hz1/2 at 2185 nm wavelength. We also found that photodetector responsivities changed by an order of magnitude with different black phosphorus orientations. This work validates black phosphorus as an effective photodetector material in the mid-IR and demonstrates the power of the glass-on-2-D-material platform for prototyping of 2-D material photonic devices.

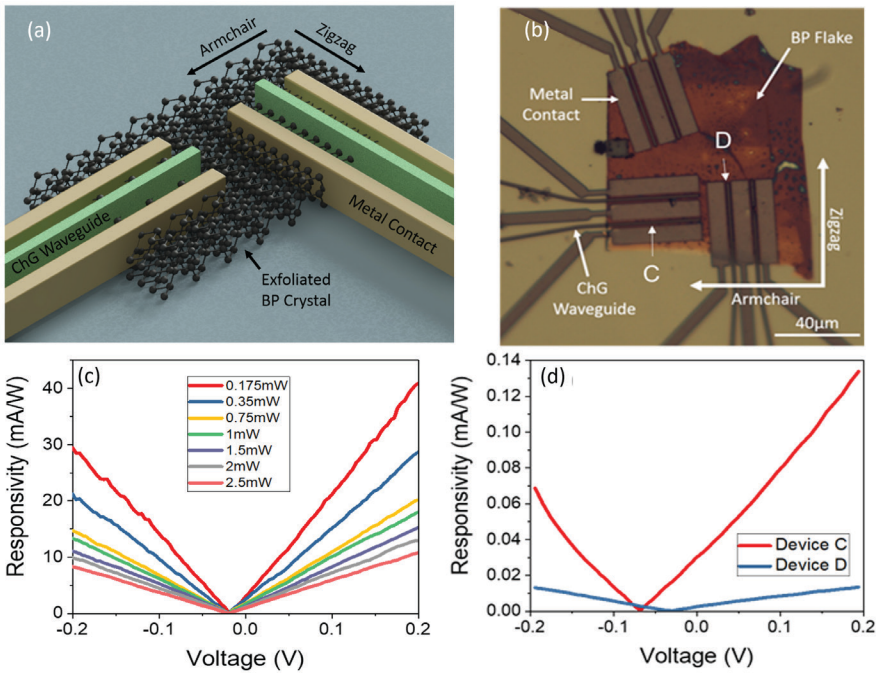

▲ Figure 1: schematic illustration of the mid-IR waveguide-integrated BP photodetectors (b) optical microscope image of mid-IR waveguide-integrated BP photodetectors (c) responsivity as a function of applied voltage at varying incident 2185 nm laser powers for a photodetector on a 32.4 nm thick flake (d) responsivities as a function of bias voltage for BP photodetectors along Armchair (Device C) and *Zigzag* direction (Device D) at 0.2 mW 2185 nm laser power.

FURTHER READING

- S. Deckoff-Jones, H. Lin, D. Kita, H. Zheng, D. Li, W. Zhang, and J. Hu, "Chalcogenide Glass Waveguide-integrated Black Phosphorus Mid-infrared Photodetectors," *J. Opt. 20*, pp. 44004, 2018.
- H. Lin, Y. Song, Y. Huang, D. Kita, S. Deckoff-Jones, K. Wang, L. Li, J. Li, H. Zheng, Z. Luo, H. Wang, S. Novak, A. Yadav, C.-C. Huang, R.-J. Shiue, D. Englund, T. Gu, D. Hewak, K. Richardson, J. Kong, and J. Hu, "Chalcogenide Glass-on-Graphene Photonics," *Nat. Photonics*, vol. 11, pp. 798–805, 2017.

An Ultrasensitive Graphene-polymer Thermo-mechanical Bolometer

Y. Lin, X. Ji, E. N. Tas, H. Cheung, J. Lang, J. Kong, T. Palacios
Sponsorship: NSF CIQM, ARO MIT-ISN

Uncooled mid-infrared (Mid-IR) detection and imaging technologies are highly desired for night vision, security surveillance, remote sensing, industrial inspection, medical, and environmental chemical sensing. Traditional mid-IR detection technologies operating at room temperature are all associated with thermal related phenomena that transfer the optical signals into electrical signals through changes of temperature on the device. Here we propose and implement a new signal transducing scheme where the energy transfer path is optical-thermal-mechanical-electrical. By combining highly sensitive strain sensors made with percolative graphene nano-flake films synthesized by Marangoni self-assembly method, and the highly efficient polymer opto-thermo-actuators, we were able to demonstrate the proof-of-concept bolometric type mid-IR detectors (Figure 1) that could be more sensitive than state-of-the-art technologies.

Two types of photoresponse behaviors were observed in our devices: a gradual change in resistance in terms of temperature (Figure 2(a)), which may be associated with the average overlap area decrease of adjacent nano-flakes; and an abrupt "switch" like response (Figure 2(b)) that is presumably due to the decrease of the number of conduction paths of the percolative film. Microscopic characterizations and theoretical modeling were carried on to understand such behaviors. Theoretical analysis showed that our new technology could be at least one order of magnitude more sensitive than the fundamental limit of existing uncooled mid-IR technologies (Figure 2(c)).

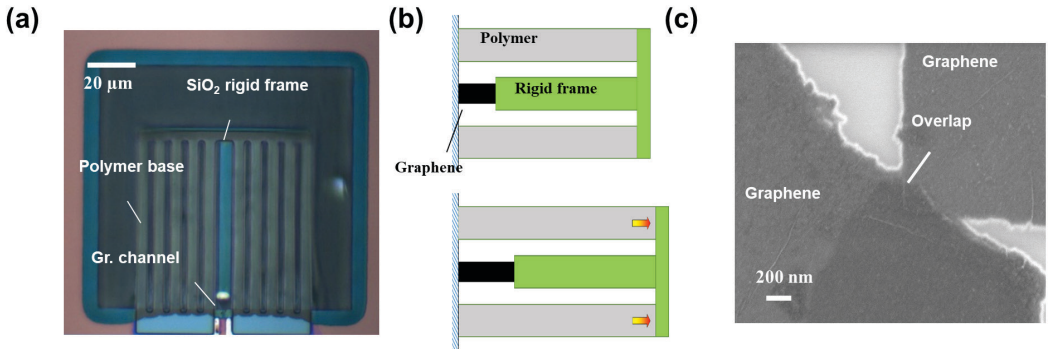

▲ Figure 1: (a) Microscopic image, and (b) Schematic of the graphene-polymer thermo-mechanical bolometer. (c) Scanning electron microscopic (SEM) image of the percolative graphene film, indicating an overlap region of around 50 nm.

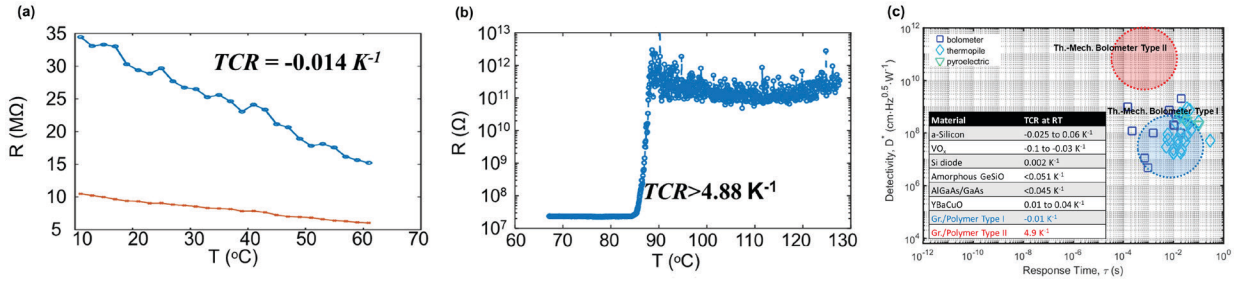

▲ Figure 2: Temperature response of the graphene-polymer thermo-mechanical bolometer, (a) Gradual change temperature dependent resistance (Type I), (b) Abrupt change temperature dependent resistance (Type II), (c) Estimated detectivities vs. response time of our devices in comparison with mainstream thermal mid-IR detectors. The inset table summarizes the typical values of temperature coefficient of resistance (TCR) of various bolometric materials.

Nanocavity Design for Reduced Spectral Diffusion of Solid-state Defects

S. Mouradian, N. Wan, M. Walsh, E. Bersin, D. Englund
Sponsorship: AFOSR

The negatively charged nitrogen-vacancy (NV) center in diamond has an electronic spin state that can be optically initialized, manipulated, and measured. Entanglement generation between two spatially separated quantum memories can be generated by coupling them to optical modes. Coupling NV centers to nanophotonic devices such as waveguides and cavities will boost the NV-NV entanglement rate by increasing the emission and collection rate of photons entangled with the spin resonators.

We can fabricate 1D photonic crystal nanobeam cavities in diamond with quality factors larger than 16,000. Unfortunately, an optimally coupled NV center in such a cavity will be only 30 nm from surfaces, and the linewidths of NV centers in such cavities is increased to 10s of GHz (1000x the natural lifetime limited linewidth) due to spectral diffusion.

To obtain NV centers with GHz linewidths in a cavity with a high-quality factor, we design and fabricate novel "Alligator" cavities. A bandgap is created via a sinusoidal width modulation. A high-Q mode is trapped in a defect created by reducing the amplitude of the modulation. The optimized mode (seen in Figure (a)) has a Q > 100,000 in simulation. We fabricate these cavities from single crystal bulk diamond. A scanning electron micrograph of one is seen in Figure (b). In experiment, we measure cavities with a mean Q value of ~7000 (Figure (d)). Figure (c) shows the spectrum of such a cavity. These structures should allow coupling between single NV centers with limited spectral diffusion and high-quality factor cavity modes.

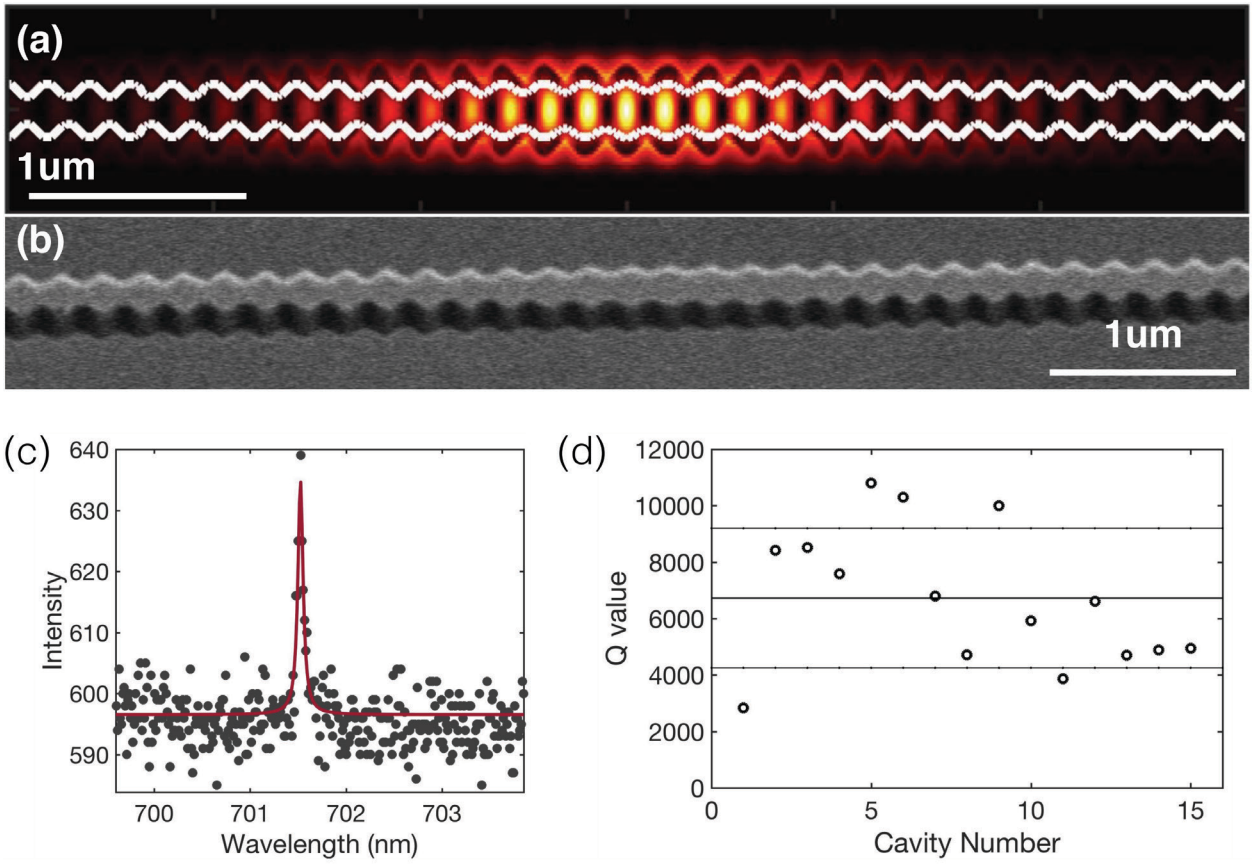

▲ Figure 1 (a) Mode profile of the optimized fundamental TE mode of an Alligator cavity. (b) Scanning electron micrograph of a fabricated Alligator cavity. (c) Spectrum of a cavity resonance (Q = 10,820). (d) Distribution of quality factors over 15 measured devices.

Two-dimensional Photonic Crystal Cavities in Bulk Single-crystal Diamond

N. H. Wan, S. Mouradian, D. Englund
Sponsorship: ARL CDQI, Master Dynamic Limited, NSF STC, NSF CIQM

Color centers in diamond are leading candidates for quantum information processing. Recent demonstrations of entanglement between separated spins of the nitrogen-vacancy (NV) color center constitute a major milestone in generating and distributing quantum information with solid-state quantum bits. However, the generation of entanglement in local quantum nodes containing NV centers is an inefficient process due to the largely incoherent NV optical transitions, as the zero-phonon-line (ZPL) constitutes only 4% of the NV's spontaneous emission. This fraction can be modified if the NV center is placed in a photonic cavity, which modifies the electromagnetic environment, and thus, the NV's emission properties via the Purcell effect. Photonic crystal (PhC) slab nanocavities offer high-quality factors (Q) and small mode volumes (V), which considerably increase the fraction of emission into the ZPL. Figure 1(A) shows the electric field profile in such a nanocavity, where the lattice constant is a = 214 nm and the thickness of the slab is H = a.

The fabrication of such structures, however, typically requires laborious reactive-ion etching (RIE) thinning of a bulk diamond down to a thickness of H. This need arises because high-quality single-crystal diamond thin films are not available and the chemically inert nature of diamond precludes wet undercutting techniques. In this work, we fabricate PhC nanocavities in diamond directly from bulk diamond. Electron beam lithography and reactive ion etching (RIE) first defines the PhC structures, after which alumina deposited using atomic layer deposition conformally coats and protects the diamond sidewalls. Then, anisotropic oxygen plasma undercuts the diamond slabs and, finally, hydrofluoric acid removes the hard mask and alumina to reveal suspended diamond structures (Figure 1(B)). We find high Q resonances near the NV ZPL wavelength of 637 nm, as shown in the photoluminescence spectra in Figure 1(C). The fabrication details and cavity measurements are in the last reference.

In conclusion, we report the first fabrication of photonic crystal slab nanocavities in bulk diamond. Immediate steps include the coherent coupling of a single NV center to the nanocavity, which will serve as a node in a quantum repeater and for solid-state cavity quantum electrodynamics investigations. This 2-D platform considerably expands the toolkit for classical and quantum nanophotonics in diamond.

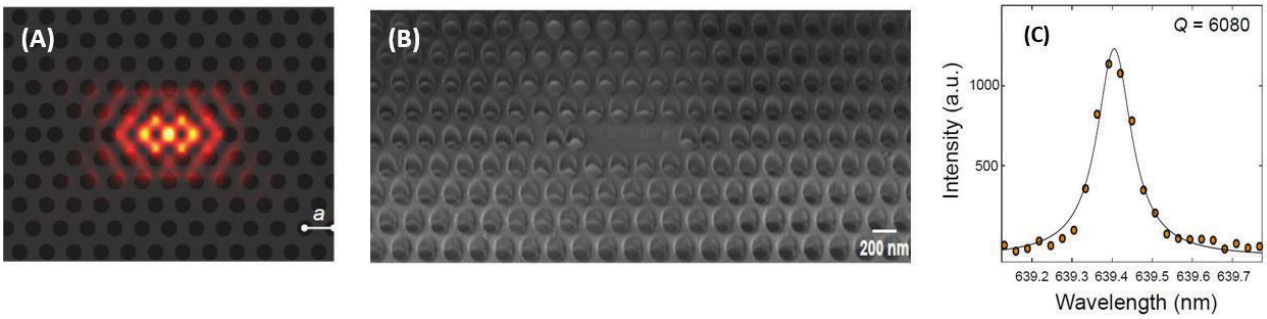

▲ Figure 1: (A) Electric field profile in an L3-defect nanocavity with a simulated Q = 8560. (B) Scanning electron microscope image of the diamond L3 nanocavity. (C) Photoluminescence spectrum of a single NV center, which reveals a high Q resonance at 639.4 nm.

FURTHER READING

- N. H. Wan, S. Mouradian, and D. Englund, "Two-dimensional Photonic Crystal Slab Nanocavities on Bulk Single-crystal Diamond," *Applied Physics Lett.* 112, pp. 141102, 2018.
- H. Bernien, B. Hensen, W. Pfaff, G. Koolstra, M. S. Blok, L. Robledo, T. H. Taminiau, M. Markham, D. J. Twitchen, L. Childress, et al., "Heralded Entanglement between Solid-state Qubits Separated by Three Metres," *Nature* 497, pp. 86–90, 2013.

Quasi-Bessel-Beam Generation using Integrated Optical Phased Arrays

J. Notaros, C. V. Poulton, M. J. Byrd, M. Raval, M. R. Watts
Sponsorship: DARPA E-PHI Program, NSF GRFP

Due to their unique diffractive properties, Bessel beams have contributed to a variety of important advances and applications, including multiplane optical trapping, reduced scattering and increased depth of field microscopy, improved laser corneal surgery, and adaptive free-space communications. Recent work has turned toward generation of Bessel beams using compact form factors, including spatial light modulators, Dammann gratings, and metasurfaces. However, these demonstrations do not provide full on-chip integration, and most are fundamentally limited to static beam formation.

In this work, integrated optical phased arrays, which manipulate and dynamically steer light, are proposed and demonstrated for the first time as a method for generating quasi-Bessel beams in a fully integrated, compact-form-factor system (Figure 1). First, the phase and amplitude distributions necessary for generating phased-array-based Bessel-Gauss beams are derived analogously to bulk-optics Bessel implementations. Next, a splitter-tree-based CMOS-compatible phased array architecture (Figure 2) is developed to passively encode arbitrary phase and amplitude feeding of the array – necessary for Bessel-Gauss-beam generation. Finally, the developed theory and system architecture are utilized to demonstrate a 0.64 mm × 0.65 mm aperture integrated phased array that generates a quasi-one-dimensional Bessel-Gauss beam with a ~14 mm Bessel length and ~30 μm power FWHM (Figure 3).

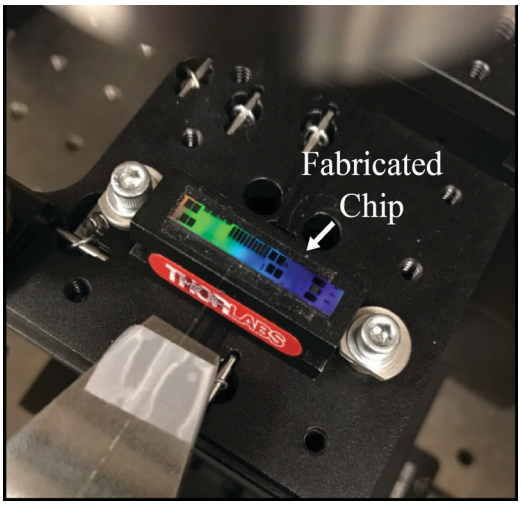

▲ Figure 1: Photograph of a fabricated integrated optical phased array chip.

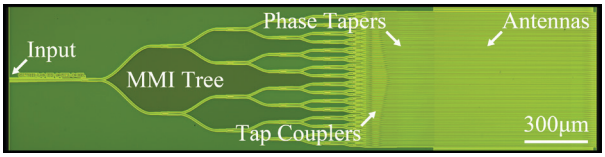

▲ Figure 2: Micrograph of the fabricated splitter-tree-based phased array showing key photonic components.

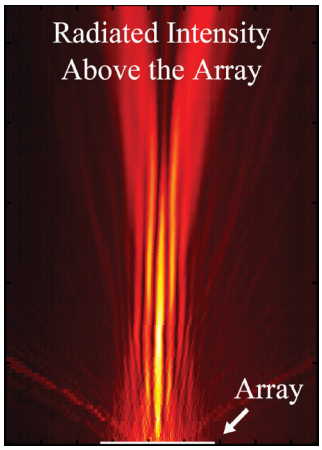

▲ Figure 3: Measured cross-sectional intensity above the quasi-Bessel-beam-generating phased array.

FURTHER READING

- J. Notaros, C. V. Poulton, M. J. Byrd, M. Raval, and M. R. Watts, "Integrated Optical Phased Arrays for Quasi-Bessel-Beam Generation," *Optics Letts.* 42, pp. 3510-3513, 2017.
- C. V. Poulton, M. J. Byrd, M. Raval, Z. Su, N. Li, E. Timurdogan, D. Coolbaugh, D. Vermeulen, and M. R. Watts, "Large-scale Silicon Nitride Nanophotonic Phased Arrays at Infrared and Visible Wavelengths," *Optics Letts.*, vol. 42, pp. 21-24, 2017.
- J. Notaros, C. V. Poulton, M. Raval, M. J. Byrd, D. Coolbaugh, and M. R. Watts, "Fresnel-Lens-Inspired Focusing Phased Arrays for Optical Trapping Applications," *Conference on Lasers and Electro-Optics. Optical Society of America*, 2017, paper STh1M.3, 2017.

See-through Light Modulators for Holographic Video Displays

S. Jolly, V. Parthiban, B. Datta, V. M. Bove, Jr.
Sponsorship: MIT Media Lab Research Consortium, AFRL

In this research (a collaboration with Dr. Daniel Smalley of Brigham Young University), we design and fabricate acousto-optic, guided-wave modulators in lithium niobate for use in holographic and other high-bandwidth displays. Guided-wave techniques make possible the fabrication of modulators that are higher in bandwidth and lower in cost than analogous bulk-wave acousto-optic devices or other spatial light modulators used for diffractive displays; these techniques enable simultaneous modulation of red, green, and blue light. In particular, we are investigating multichannel variants of these devices with an emphasis on maximizing the number of modulating channels to achieve large total bandwidths. To date, we have demonstrated multichannel full-color modulators capable of displaying holographic light fields at standard-definition television resolution and at video frame rates. Our current work explores a device architecture suitable for wearable augmented reality displays and other see-through applications, in which the light outcouples toward the viewer (Figure 1), fabricated using femtosecond laser micromachining (Figure 2).

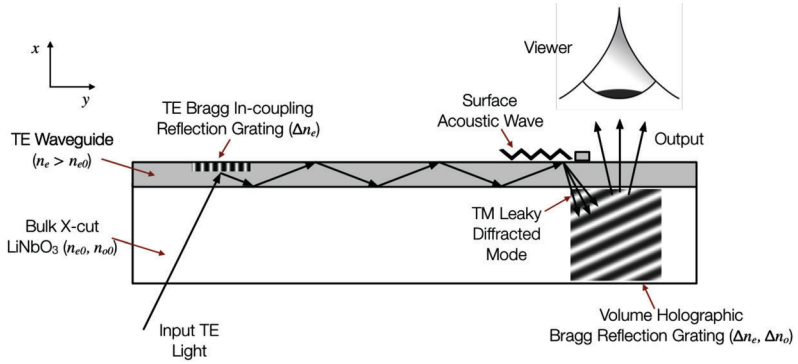

▲ Figure 1: Diagram of near-eye version of our device.

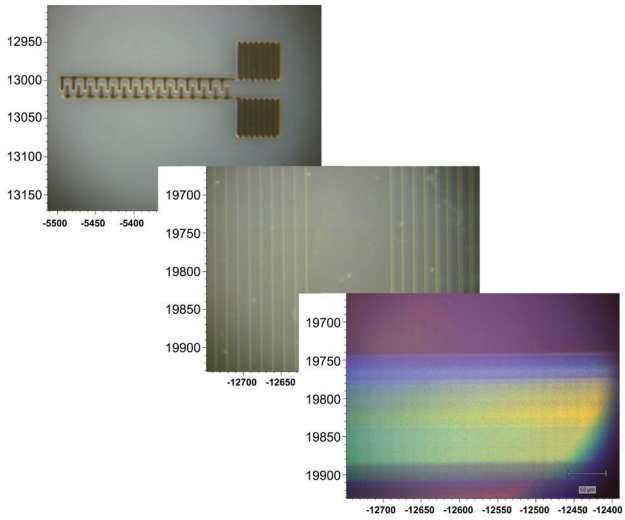

▲ Figure 2: Metal features, waveguides, and reflection gratings fabricated using femtosecond laser processing.

FURTHER READING

- S. Jolly, N. Savidis, B. Datta, D. Smalley, and V.M. Bove, Jr., "Progress in Transparent, Flat-panel Holographic Displays Enabled by Guided-wave Acousto-optics," *Proceedings SPIE Practical Holography XXXII: Displays, Materials, and Applications*, pp. 10558, 2018.
- S. Jolly, N. Savidis, B. Datta, T. Karydis, w. Langford, N. Gershenfeld, and V. M. Bove, Jr., "Progress in Fabrication of Anisotropic Bragg Gratings in Lithium Niobate via Femtosecond Laser Micromachining," *Proceedings SPIE Advanced Fabrication Technologies for Micro/Nano Optics and Photonics XI*, pp. 10554, 2018.

A Scalable Single-photon Detector Array Based on Superconducting Nanowires

D. Zhu, Q.-Y. Zhao, H. Choi, T.-J. Lu, A. E. Dane, D. R. Englund, K. K. Berggren
Sponsorship: AFOSR, DARPA, NSF

Detecting single photons over large numbers of spatial modes is crucial for photonic quantum information processing. This measurement usually requires an array of time-resolved single-photon detectors. The superconducting nanowire single-photon detectors (SNSPDs) are currently the leading single-photon counting technology in the infrared wavelength and have the highest performance in timing jitter, detection efficiency, and counting rate. In a conventional readout scheme, each SNSPD requires one coaxial cable in the cryostat, a low-noise RF amplifier, and a high-resolution time-to-digital converter. Implementing a system of a few SNSPD channels with the conventional readout is possible, but scaling them to tens or hundreds of channels requires formidable resources and remains an outstanding challenge.

Here, we report a scalable two-terminal SNSPD array that only requires one pair of RF cables for the readout. Figure 1 shows the architecture of the array, where a chain of detectors was connected using superconducting nanowire delay lines. The nanowire delay lines were designed to be slow-wave transmission lines with a phase velocity of only 0.016c, where c is the speed of light in vacuum. When a detector absorbs a photon and fires, it generates a pair of counter-propagating pulses towards the two terminals. By registering the pulses on the two terminals, and performing simple timing logic, one can resolve the arrival locations of up to two incident photons (see Figure 2). By analyzing the electrical pulse shapes, we also showed photon-number-resolving capability in a 4-element device. This device architecture will be useful for multi-photon coincidence detection in photonic integrated circuits.

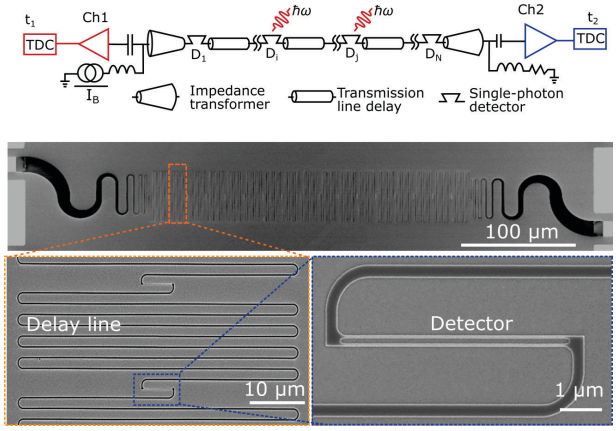

▲ Figure 1: Device architecture. Top: Equivalent circuit diagram of the device, where detectors are connected using delay lines and read out on both terminals. Bottom: Scanning electron micrograph of a 16-element array.

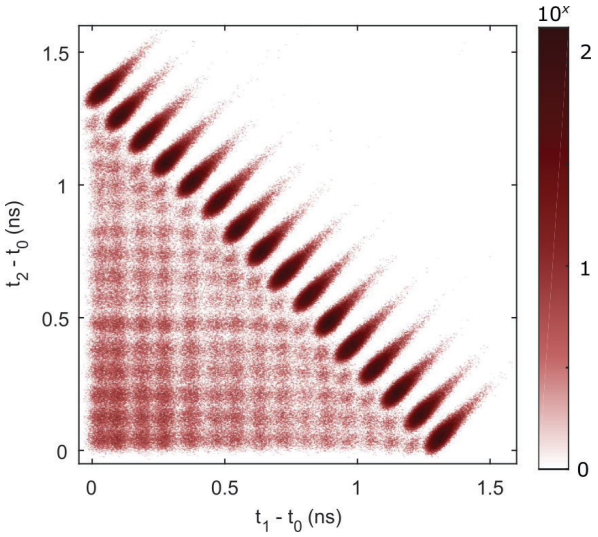

▲ Figure 2: A histogram constructed from 1 million detection events from the 16-element detector array. t_0: photon arrival time; t_1 and t_2: electrical pulse arrival time at Ch1 and Ch2.

FURTHER READING

- D. Zhu, Q.-Y. Zhao, H. Choi, T.-J. Lu, A. E. Dane, D. Englund, and K. K. Berggren, "A Scalable Multi-photon Coincidence Detector Based on Superconducting Nanowires," *arXiv:1711.10546*, 2017.
- Q.-Y Zhao, D. Zhu, N. Calandri, A. E. Dane, A. N. McCaughan, F. Bellei, H.-Z. Wang, D. F. Santavicca, and K. K. Berggren, "Single-photon Imager Based on a Superconducting Nanowire Delay Line," *Nature Photonics*, vol. 11, no. 4, pp. 247, 2017.
- N. Calandri, Q.-Y. Zhao, D. Zhu, A. E. Dane, and K. K. Berggren, "Superconducting Nanowire Detector Jitter Limited by Detector Geometry," *Applied Physics, Lett.*, vol. 109, no. 15, pp. 152601, 2016.

Utilization of $BaSnO_3$ and Related Materials Systems for Transparent Conducting Electrodes

M. Campion, S. R. Bishop, H. L. Tuller
Sponsorship: NSF

Efficient, transparent electrode materials are vital for applications in smart window, LED display, and solar cell technologies. These materials must possess a wide band gap for minimal optical absorption in the visible spectrum while maintaining high electrical conductivity. Tin-doped indium oxide (ITO) has been the industry standard for transparent electrodes, but the use of the rare element indium has led to a search for better material alternatives. $BaSnO_3$ represents a promising alternative due to its high electron mobility and resistance to property degradation under oxidizing conditions, but the mechanisms by which processing conditions and defect chemistry affect the final material properties are not well understood.

This work seeks to better understand the relationships between processing, defect chemistry, and material properties of $BaSnO_3$, to better establish the consistent and controllable use of $BaSnO_3$ as a transparent electrode. To accomplish these goals, methods such as *in situ* resistance and impedance monitoring during annealing will be applied. In addition, a variety of novel methods such as the *in situ* monitoring of optical transmission (shown in Figure 1) during annealing and the *in situ* monitoring of resistance during physical vapor deposition will be utilized to investigate $BaSnO_3$. Direct measurements of the key constants for the thermodynamics and kinetics of oxidation in donor-doped $BaSnO_3$ will be experimentally determined for the first time. This increase in understanding will provide a predictive model for determining optical properties, carrier concentrations, and electron mobilities in $BaSnO_3$, which may be become increasingly important due to its high electron mobility, high-temperature stability, and favorable crystal structure.

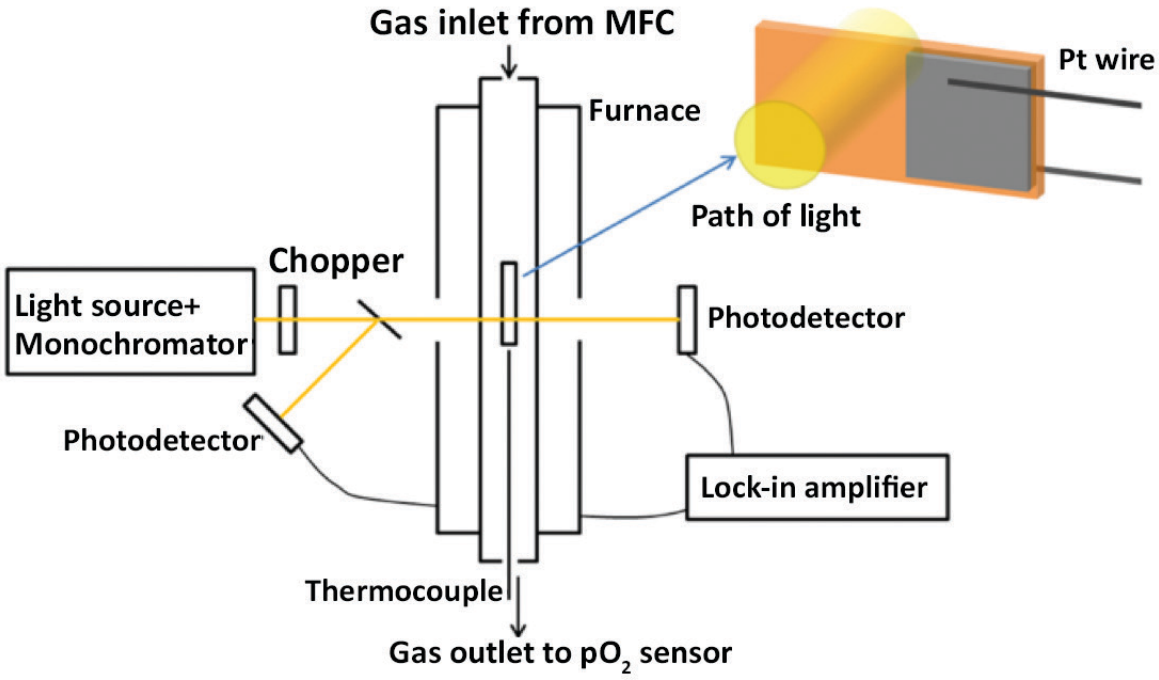

▲ Figure 1: Schematic of an experimental setup to be used for simultaneous *in situ* measurement of the optical transmission and electrical conductivity of thin film $BaSnO_3$ samples during annealing under controlled atmosphere and temperature.

FURTHER READING

- J. J. Kim, S. R. Bishop, N. J. Thompson, D. Chen, and H. L. Tuller, "Investigation of Nonstoichiometry in Oxide Thin Films by Simultaneous *in situ* Optical Absorption and Chemical Capacitance Measurements: Pr-Doped Ceria, a Case Study," *Chemistry of Materials*, vol. 26, no.3, pp. 1374-1379, 2014.
- D. O. Scanlon, "Defect Engineering of BaSnO3 for High-performance Transparent Conducting Oxide Applications," *Phys. Rev. B,* vol. 87, no. 16, pp. 161201, Apr. 2013.